Materials Today: Proceedings 65 (2022) 3348–3356

Contents lists available at ScienceDirect

Materials Today: Proceedings

journal homepage: www.elsevier.com/locate/matpr

Optimization and thermal analysis of friction stir welding on AA6061 aluminum alloys

Lingerew E. Melaku *, Amanuel D. Tura, Hana B. Mamo, A. Johnson Santhosh, N. Ashok

Faculty of Mechanical Engineering, Jimma Institute of Technology, Ethiopia

ARTICLE INFO

Article history:
Available online 6 June 2022

Keywords:
Temperature
CEL
ABAQUS
Friction stir welding
Thermal analysis
Defects

ABSTRACT

This research focuses on the thermal analysis and optimization of FSW AA 6061 alloy joints at various welding speeds, rotational speeds, and tool geometry. Tool shoulder (concave and flat) and tool probe (tapered and cylindrical) geometries were used to weld a workpiece. The aim of this paper is to get a defect free joint by optimizing temperature using finite element analysis. A Coupled Eulerian-Lagrangian (CEL) approach on ABAQUS software was used to simulate butt joints to study thermal phenomena and defects such as tunnel, flash, and crack formation during FSW. The temperature range for welding was found via software simulation. Experimental work validated the temperature value obtained from finite element analysis. Based on the Taguchi L9 orthogonal array, nine tests were done and optimized. A Dual Laser InfraRed thermometer was used to measure the temperature of the welded workpiece. To obtain accurate results in FE, the quality of mesh was evaluated using trial and error procedures. The numerical analysis results were in good accord with the experimental data. A concave shoulder tool with tapered probe gives a defect free joint at 1000 rotational speed and 20 mm/min welding speed. The maximum temperature of 560 °C was observed when concave shoulder with tapered probe was used at 1200 rotational speed and 15 mm/min welding speed.

1. Introduction

W.Thomas and E. Nicholas invented friction stir welding (FSW) at The Welding Institute (TWI) Cambridge, in 1991[1,17]. FSW is used for joining similar and dissimilar metals [2]. Friction-Stir Welding can join metals that are hard to weld using fusion welding. Aluminium alloys, copper and its alloys, mild steel, stainless steel, and magnesium alloys are the most common metals, welded using FSW. Even though FSW was invented for soft metals, nowadays, this technique has a wide application such as in trains, aerospace, the automobile, marine, etc.[3].

A non-consumable rotating tool with a shoulder and probe at one end is used to soften the material due to friction between the tool shoulder and the workpiece. Material flow and heating are characterized by contact conditions at the interface between the tool shoulder and workpiece, classified as sliding, sticking, or both sliding and sticking [4]. The friction between shoulder and workpiece generates heat as a tool rotates from advancing to retreating side. The tool-workpiece interface of FSW under butt joint is shown in Fig. 1. According to Coulomb's law, the coefficient of friction is a constant variable and depends on temperature, but is considered kinetic friction only when the contact conditions are non-sticking [5]. The total heat generation and plastic deformation of the workpiece is considered a combination of sliding friction and adhesive friction [6].

$$dQ_{FSW} = dQ_f + dQ_s = (1-\delta)\omega r \mu p dA + \delta\omega r \frac{\sigma_y}{\sqrt{3}} dA \quad (1)$$

The mechanical interaction between the rotating welding tool and the stationary workpiece generates heat by applied pressure and friction. Different design features of the tool and shoulder vary the amount of heat generation and stirring material. There are three surfaces of the tool that are used as a source of heat generation by friction and enable the joining of weld pieces [7]. These are the tip of the probe, lateral surface of the probe, and face of the shoulder. In the present analysis, three different tool geometries were used. A shoulder face (flat and concave) and probe (tapered

* Corresponding author.
E-mail addresses: lingerw.enbakom@ju.edu.et (L.E. Melaku), diriba.amanuel@ju.edu.et (A.D. Tura), hana.beyene@ju.edu.et (H.B. Mamo), johnson.antony@ju.edu.et (A. Johnson Santhosh), nagaraj.ashok@ju.edu.et (N. Ashok).

https://doi.org/10.1016/j.matpr.2022.05.463
2214-7853/

Nomenclature

H_p	*Length of pin*	δ	*Extent of sticking*
Q_T	*heat generation by pin tip surface*	T_c	*Contact shear stress*
Q_p	*Heat generation by pin lateral surface*	T_y	*contavt yield stress*
Q_s	*Heat generation by shoulder surface*	ω	*radial velocity*
α	*pin taper angle*	σ_y	*Yield stress*
θ	*concave angle*		

and straight cylindrical) were used. Heat generation is mainly influenced by taper angle, concave angle, and diameters. The governing equation of heat generation due to probe tip (Q_T), probe surface (Q_p) and shoulder surface (Q_s) are given by the equations (2), (3) and (4), respectively.

$$\boldsymbol{Q_T = \frac{2}{3}\pi\tau_c\omega R_t^{\,3} = \frac{2}{3}\pi\omega\left[\delta\tau_y + (1-\delta)\mu p 3\right]R_t^{\,3}} \tag{2}$$

$$\begin{aligned}\boldsymbol{Q_p} &= \boldsymbol{\frac{2}{3}\pi\tau_c\omega\left(R_p^{\,3} - R_t^{\,3}\right)\left(\frac{1+\tan\alpha}{\tan\alpha}\right)} \\ &= \boldsymbol{\frac{2}{3}\pi\omega\left[\delta\tau_y + (1-\delta)\mu p 2\right]\left(R_p^{\,3} - R_t^{\,3}\right)\left(\frac{1+\tan\alpha}{\tan\alpha}\right)}\end{aligned} \tag{3}$$

$$\begin{aligned}\boldsymbol{Q_s} &= \boldsymbol{\frac{2}{3}\pi\tau_c\omega\left(R_s^{\,3} - R_p^{\,3}\right)(1+\tan\theta)} \\ &= \boldsymbol{\frac{2}{3}\pi\omega\left[\delta\tau_y + (1-\delta)\mu p 1\right]\left(R_s^{\,3} - R_p^{\,3}\right)(1+\tan\theta)}\end{aligned} \tag{4}$$

Some researchers have been working on optimization of FSW for different materials using both experimental and numerical methods [1,8]. However, the quality of FE analysis is not good enough in most research results due to improper mesh optimization. Identifying the reason of defect formation in FSW joint plays a big role to ensure the quality. Narges Dialami et al. [9] studied the defect formation such as flash, voids, wormholes and joint using cylindrical and threaded tool. Fashami Hoda et al [10] tried to produce a defect free joint on AZ91 material using at different rotational and welding speed. The present study showed the material flow around the weld nugget zone using ABAQUS software by varying tool geometry, welding speed, and rotational speed at a better mesh quality. This paper tried to find the defect on joint at different rotational, welding speed and tool geometry on AA6061-T6. The aim of this study is checking mesh quality, defect formation reason and effect of temperature on weld quality.

The paper is outlined as follows. In section 2, materials and methods of FSW modelling are briefly described. In this section, the use of CEL technique for thermal analysis and experimental works are addressed. In section 3, results and discussions about the temperature results from numerical and experimental and defects analysis are included. Section 4 summarizing the effect of each parameters on the final temperature and defect formation.

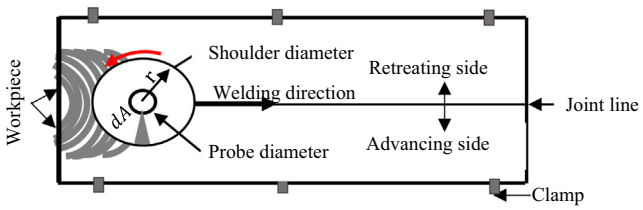

Fig. 1. Tool-work interface.

2. Materials and methods

The analysis of thermal phenomena in FSW was examined in numerical method and experimental investigation. Numerical analysis is a cost-effective method, but less accurate than experimental due to many assumptions considered in FE. Many researchers have done numerical analysis using different software. Among this software, Abaqus is widely used by enormous researchers due to its capabilities to perform FEM. ABAQUS is used to perform the simulations and analysis of FSE estimate stress, temperature, heat transfers, and bulk deformations [8]. Although the software by itself can perform both mechanical and thermal aspects, the accurateness of the result is still questionable due to the user knowledge gap. This research work contributes to the scientific advancement of FE analysis using appropriate software to develop a thermo-mechanical model with a major novelty. In this study, the numerical result assures by optimizing mesh quality.

2.1. Thermal analysis using coupled eulerian-lagrangian (CEL)

ABAQUS is suitable software for Finite Element (FE) analysis of friction stir welding and has proven to be a cost-effective tool for the prediction of various output responses without having experimental trails or a physical product [11]. Numerical modelling of FSW attempts to predict weld phenomena, like temperature, material flow properties, and defect formation [12]. The friction stir welding process involves excessive deformations and heat generation on a workpiece that is difficult to simulate and solve using the classical FE method. The convergent solution cannot be obtained due to large deformations, mesh distortions, and contact problems that occur on the tool-workpiece interface. CEL method should be used in ABAQUS/explicit to reduce those difficulties concerning large deformation [13]. CEL has capable of obtaining certain insights such as temperature, heat generation, flash formation, the extent of mixing from advancing side to retreating side, and formation of defects.

In the present study, ABAQUS_2017 was employed to simulate the FSW in different tool geometry. Characterization of weld joint is dependent on the material flow and extent of plastic deformation. Material which to be weld is under high deformation and high temperature in heat affected zone due to frictional heat between work and tool. The extent of deformation and amount of heat generation is obviously, influenced by the tool geometry and other process parameters [17].

The CEL analysis technique is a method in which both Lagrangian and Eulerian elements should combine in the same model. In a CEL analysis, bodies that will have excessive deformations must mesh with Eulerian elements. Stiffer bodies, tools, meshed with Lagrangian elements. In this technique, the workpiece is considered as Eulerian elements while the tool is Lagrangian elements. The main advantage of using this CEL analysis technique is to eliminate mesh distortion due to high deformation. The coupled eulerian lagrangian FE method exhibited a potential of defect prediction around the welded nugget zone, which ultimately can help process parameters optimization.

It also helps to reduce a computational time to a significant amount thereby making FE simulations will do in minimum memory [14,13]. A series of steps in FE simulation of FSW includes part drawing, assembly, property definition, interaction, boundary condition, mesh, and job.

The first step in FE analysis is geometry creation/part drawing. The tool geometries are cylindrical probe, tapered probe, flat shoulder and concave shoulder as shown Fig. 2. The geometry of the welded specimen is modelled by using the commercial software package, ABAQUS/explicit. This specimen consists of two 6061 aluminum alloy plates with dimensions 500 × 100 × 2 mm each. The 3D model consists of one eulerian, lagrangian, and welding tool. Lagrangian is model as 3D, deformable solid part, unlike eulerian is as 3D eulerian.

The second step is adding material properties and section assignments based on the required material. ABAQUS has no built-in units system, and therefore, all input mechanical and thermal properties should be specified in consistent units. All the properties of AA6061 should be properly added to the property module. The units used for the analysis are always the same in the ABAQUS environment for both workpiece and tool material in the analysis. In this analysis, a system of units of « mm, N, tone, sec » is used as shown in Table 1.

All the required properties of AA-6061 alloy are given in Table 4. Material properties were added based on the Johnson-Cook model, Eq. (1), flow stress(σ) as a function of strain hardening rate and temperature [15,16].

$$\boldsymbol{\sigma} = (\boldsymbol{A} + \boldsymbol{B}\boldsymbol{\varepsilon}^{\boldsymbol{n}})[1 + \boldsymbol{C}\ln\left(1 + \frac{\boldsymbol{\varepsilon}}{\boldsymbol{\varepsilon_o}}\right)\left(1 - \left[\frac{\boldsymbol{T} - \boldsymbol{T_{room}}}{\boldsymbol{T_{melt}} - \boldsymbol{T_{room}}}\right]\right) \quad (5)$$

Where, T_{melt}– melting point, T_{room} room temperature, T– temperature, A - yield stress, B– strain factor,n– strain exponent, m– temperature exponent, $\frac{\varepsilon}{\varepsilon_o}$– plastic strain and C– strain rate factor.

The third step in Abaqus FE analysis is the assembly module. In this step Eulerian, Lagrangian and tool are assemble as shown in Fig. 3. The center of the tool probe should be exactly aligned to the contact line of the two joining plates. A small distance is provided between the tooltip and the surface of the workpiece during assembly.

FSW processes include plunging, dwelling, and welding steps. After assembling all the parts, the step time is given for plunging, dwelling, and welding. In the plunging step, the tool rotates and moves downward, and penetrates the workpiece on the contact line due to applied pressure exerted by the machine spindle. After proper penetration, the tool will stop downward movement and rotate at that position. This duration of time is known as dwelling time. Dwelling is a duration of time sufficient to plasticize the material. Moreover, welding time is the length of time from the end of the dwelling to the end of welding. The analysis procedure is *"Dynamic, Temp-disp, explicit"* type because this numerical study contains thermal and mechanical aspects. Output variables such as nodal temperature, stress, and contact energy will examine from the field output request.

Discretization or mesh is a very determinant issue in the FE analysis procedure. Mesh size is one of the most influential parameters in FEA result accuracy. A bigger element size gives inaccurate results. Unlike, fine mesh gives accurate results but computational time is much longer than coarse mesh. The main challenges are finding the correct mesh size to get an accurate result with minimum possible computing time. One of the most important issues in FE analysis that affects result accuracy is mesh type and compatibility. Since the results are mesh-dependent, mesh quality should be maintained in both workpiece and tool models to ensure result

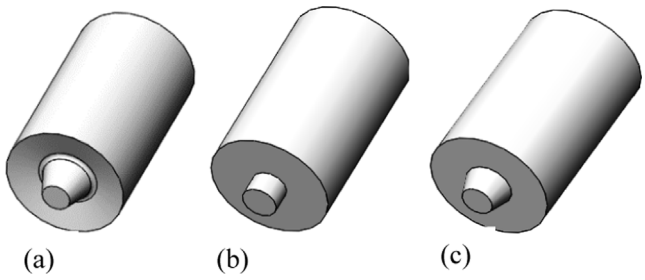

Fig. 2. Tool geometries (a) Concave, taper probe (b) Flat, cylindrical probe and (d) Flat, taper probe.

Table 1
Set of units [8].

Quantity	SI	SI (mm)	US Unit(ft)
Length Force Mass Time Stress Energy Density	mNKgsPa(N/m^2)JKg/m^3	mmNTonne(10^3 kg)sMPa (N/mm^3)mJ(10^{-3}J)tonne/mm^3	Ftlbfslugslbf/ft^{2}ft. lbfslug/ft^3

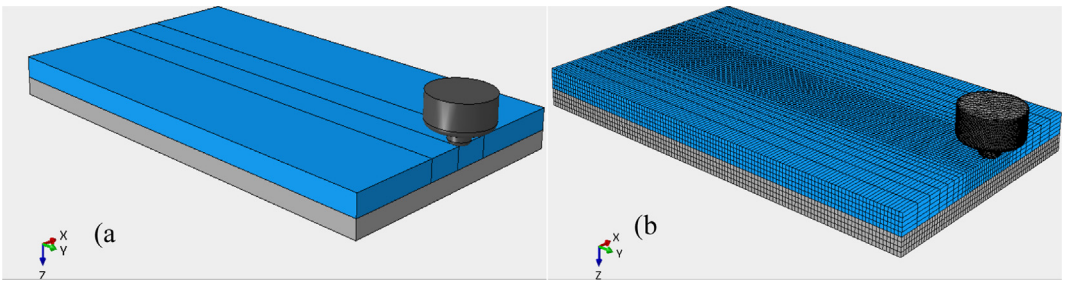

Fig. 3. 3D model of tool-workpiece assembly (a) Eulerian-Lagrangian assembly (b) mesh.

convergence. The optimum mesh size can be obtained by trial and error techniques. Firstly, analysis is submitted in coarse mesh and the result will be recorded. Secondly, mesh size was reduced and submitted for analysis and the different results obtained, and so on. Finally, the result of a particular mesh size will be almost similar to the former as shown in Fig. 4. The stress-induced at a mesh size of 0.4 is almost equal to the result in mesh size of 0.333 as shown in Table 2. The resulting accuracy will no longer have a significant change if more refinement is performed but the computation time will increase significantly.

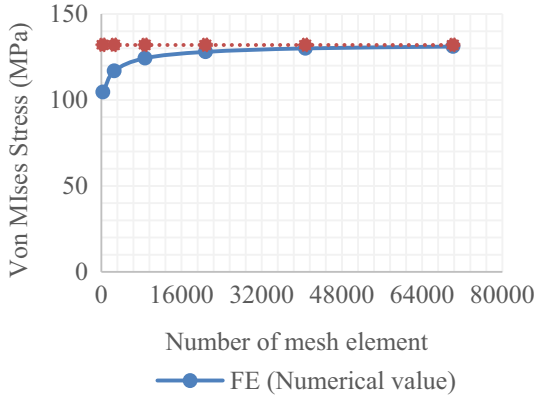

Fig. 4. Optimum mesh size plot.

Table 2
Mesh optimization.

	Mesh size	Elements	Max Von misses (Mpa)
mesh 0	2	330	104.54
mesh1	1	2600	116.85
mesh2	0.6667	8730	124.31
mesh3	0.5	20,800	127.98
mesh4	0.4	40,750	130.02
Mesh5	0.333	70,200	131.07

Table 3
Process parameters combination.

Exp. No.	Welding speed (mm/min)	Rotation speed (rpm)	Tool geometries
1	10	750	Concave shoulder, taper probe
2	15	750	Flat shoulder, cylindrical probe
3	20	750	Flat shoulder, taper probe
4	10	1000	Flat shoulder, cylindrical probe
5	15	1000	Flat shoulder, taper probe
6	20	1000	Concave shoulder, taper probe
7	10	1200	Flat shoulder, taper probe
8	15	1200	Concave shoulder, taper probe
9	20	1200	Concave shoulder, cylindrical probe

2.2. Experimental work

The Design of Experiments (DOE) is a statistical method that tries to offer a predictive understanding of a complex, multivariable procedure with few trials [19]. After modelling and simulation, experiments will perform on the proposed materials to compare software and experiment results. Taguchi experimental design method was applied to decide the minimum experimental tests in 3 levels and 3 factors. Those numbers of experiments were performed by three different process parameters; rotation speed, welding speed, and tool geometry to show the effect on the response variables of *peak temperature* and *defect formation* on welded joint. The numerical value and the combination of all three-process parameters are given in Table 3. Welding was performed on vertical milling machine Fig. 5.

In the present work, an aluminum alloy of AA6061 is a workpiece material. Magnesium and silicon are the principal alloying elements in AA6061 and are commonly used for architectural extrusions and auto- motive components. The tool should model as a discrete rigid body to reduce computational time. The main objective in this analysis is to show a temperature contour on the workpiece but the temperature on the tool is not considered.

Fig. 5. FSW processes on AA6061.

Table 4
Mechanical and thermal properties of aluminum alloy (AA6061) based on the Johnson-cook plasticity model [18].

Properties	Symbol	Value	Properties	Symbol	Value
Density	ρ	$2690 kg/m^3$	Strain hardening parameter	B	$114 MPa$
Specific heat	C_p	$945\ J/kg.^{\circ}C$	Strain rate coefficient	C	0.002
Thermal Conductivity	K	$167 W/m^{\circ}C$	Strain hardening exponent	n	0.42
Young's Modulus	E	$66.94 Gpa$	Room temperature	T_{room}	$25^{\circ}C$
Poisson ratio	υ	0.33	Temperature exponent	m	1.34
Yield Strength	σ_y	$240 Mpa$	Melting temperature	T_{melt}	$660^{\circ}C$
Reference Strength	A	$324 MPa$			

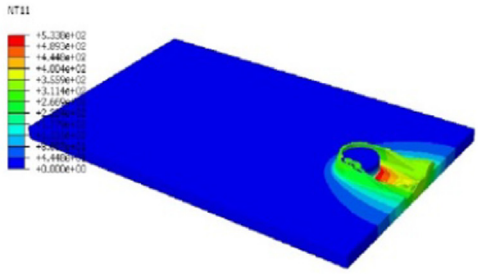

a) 750 rpm, 10mm/min, Concave shoulder with taper probe probe

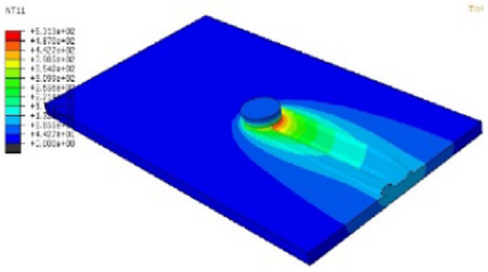

b) 750 rpm, 15mm/min, Flat shoulder with cylindrical

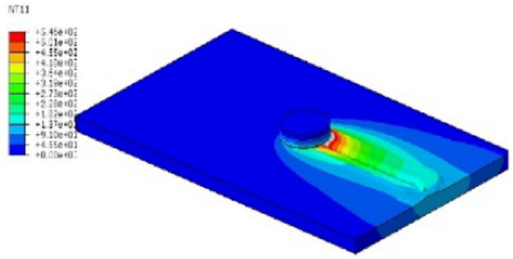

c) 750 rpm, 20mm/min, Flat shoulder with taper probe

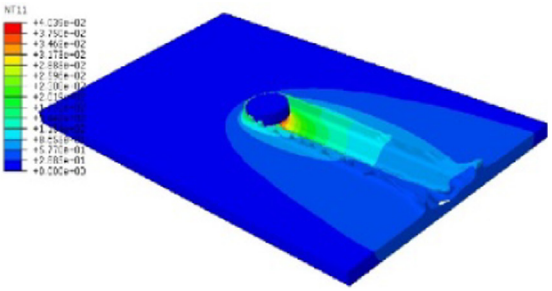

d) 1000 rpm, 10mm/min, Flat shoulder with cylindrical probe

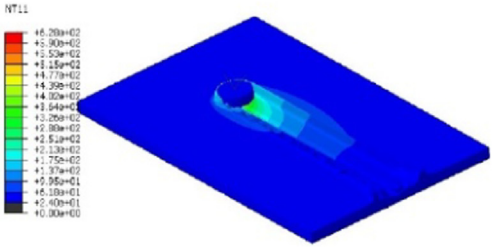

e) 1000 rpm, 15mm/min, Flat shoulder with taper probe

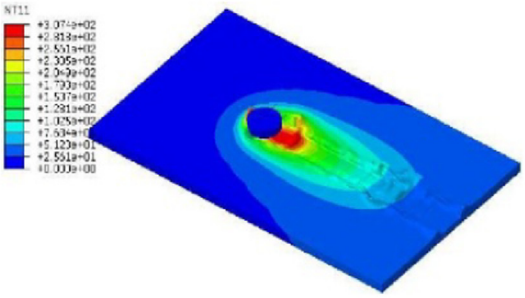

f) 1000 rpm, 20mm/min, Concave shoulder with taper probe

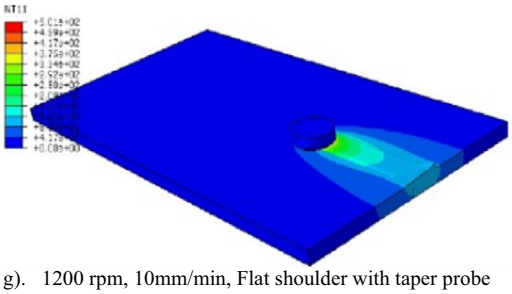

g). 1200 rpm, 10mm/min, Flat shoulder with taper probe

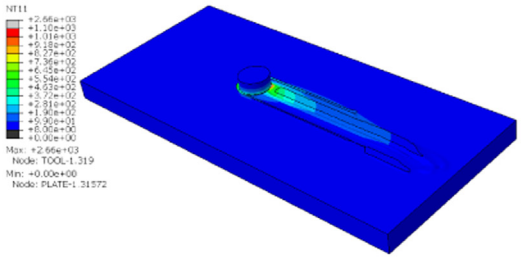

h) 1200 rpm, 15mm/min, Concave shoulder with taper probe

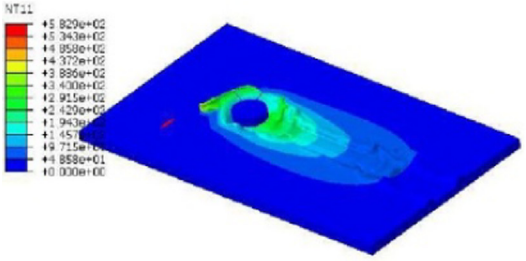

i) 1200 rpm, 20mm/min, Flat shoulder with cylindrical probe

Fig. 6. (a–i). Nodal temperature contour in FSW.

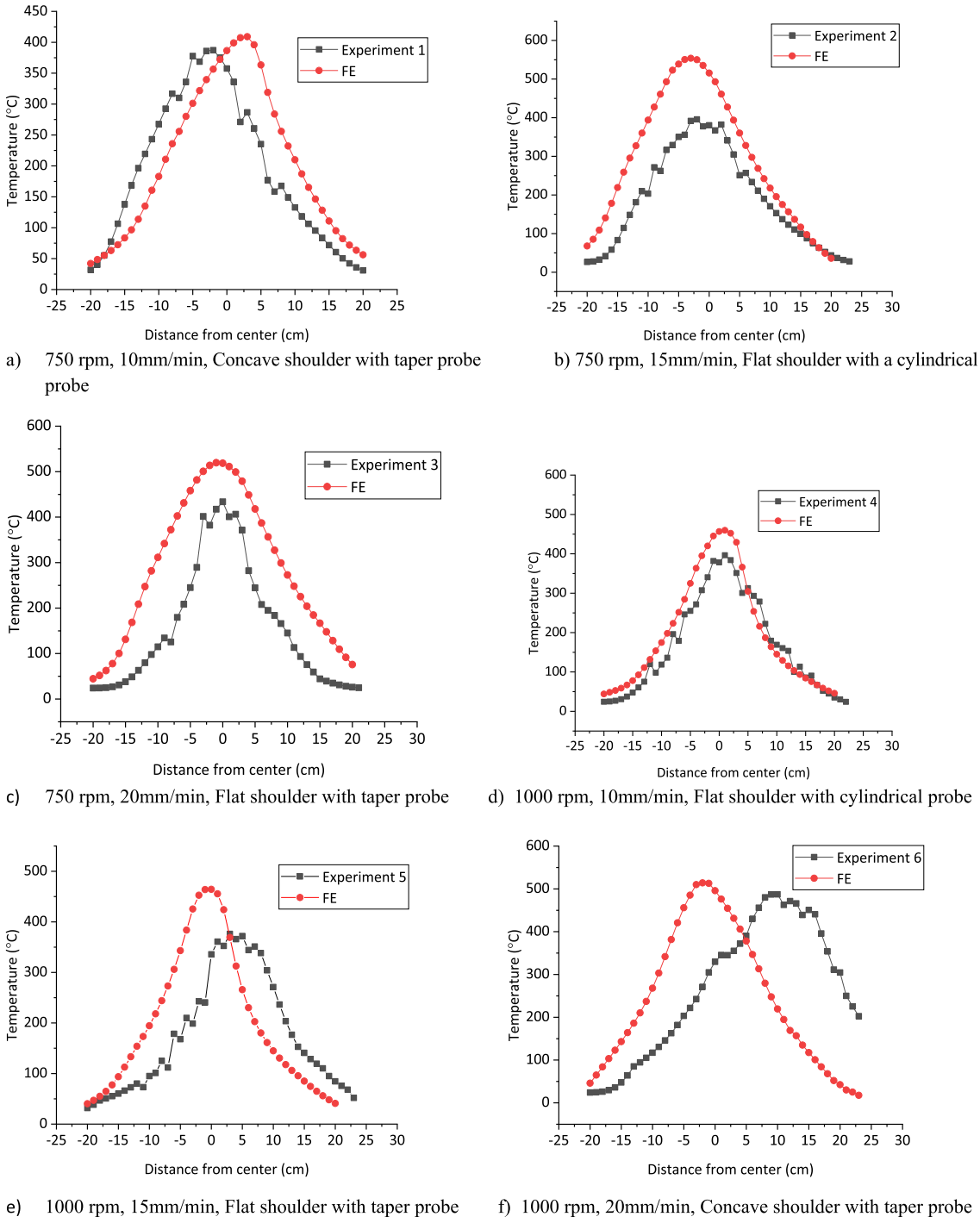

a) 750 rpm, 10mm/min, Concave shoulder with taper probe probe

b) 750 rpm, 15mm/min, Flat shoulder with a cylindrical

c) 750 rpm, 20mm/min, Flat shoulder with taper probe

d) 1000 rpm, 10mm/min, Flat shoulder with cylindrical probe

e) 1000 rpm, 15mm/min, Flat shoulder with taper probe

f) 1000 rpm, 20mm/min, Concave shoulder with taper probe

Fig. 7. (a–i). Temperature plot across the width of the plate.

3. Results and discussions

3.1. Numerical and experimental temperature

The most important assessment to confirm the accuracy of FE analysis in the FSW process focuses on the temperature contour [8]. The peak temperature varies with tool shoulder diameter, material property, rotational speed, workpiece thickness, probe geometry, shoulder face profile, welding speed, etc. The maximum temperature (550°C) in the FE analysis was observed on a flat shoulder with the cylindrical probe at 750 rpm rotational speed and 15mm/min. welding speed, Fig. 6. In addition, maximum temperature (560 °C) was observed at 1200-rpm rotational speed, concave shoulder with taper probe and 15mm/min. welding speed. The shoulder face had a great effect on temperature value. More than 80% of the total heat generation is from the shoulder features and 14–17% of heat is generated by probe [20]. The numerical and experimental values of temperature are given in Fig. 7 across the width of the sheet. The maximum temperature recorded on the surface is at the center of the joint line, the nugget zone.

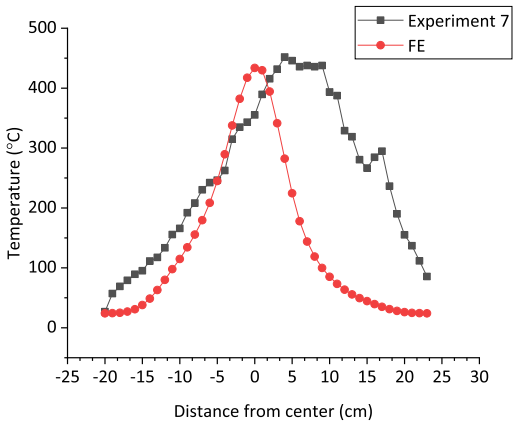

g) 1200 rpm, 10mm/min, Flat shoulder with taper probe

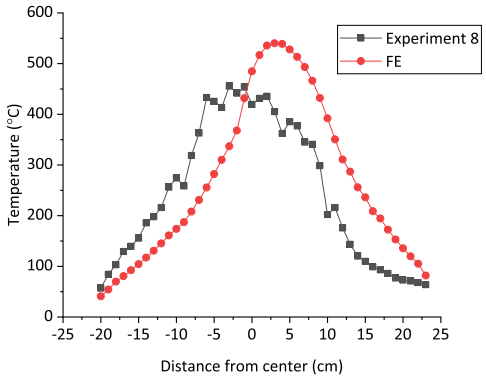

h) 1200 rpm, 15mm/min, Concave shoulder with taper probe

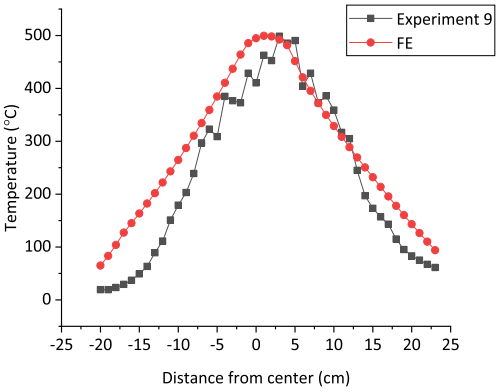

i) 1200 rpm, 20mm/min, Flat shoulder with a cylindrical probe

Fig. 7 (*continued*)

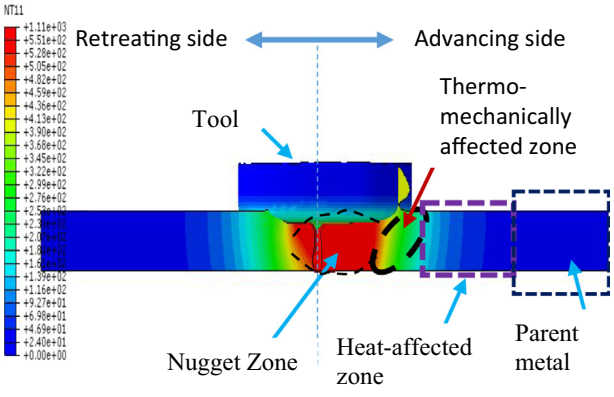

Fig. 8. Thermomechanical zone.

3.2. Defect analysis

Examination of the microstructure showed that the weld defects, tunnel, void, crack, etc. can be seen around the.

weld nugget zone [21]. The present study confirmed the existence of defects on the FSW joint and the most influential parameters were determined. The temperature had a considerable effect on the formation of defects. As shown in Fig. 8, the plasticized region around the tool probe consists of high heated material, nugget zone. In this nugget zone, the material grains will be dynamically recrystallized and highly distorted but in the adjacent thermomechanically affected zone, some not recrystallized grains are present Fig. 8. This recrystallization variation causes a crack defect. Tunnel defect formed when the temperature is high and higher welding speed causes crack due to rapid cooling of joint. The observed defects and values of temperatures are tabulated below for all process parameters combination, Table 5. Defects

Table 5
Temperature results and observed defects.

Exp. No.	Welding speed (mm/min)	Rotation speed (rpm)	Tool geometries	Max. Temperature (°C)		Observed defect
				Experimental	Numerical	
1	10	750	Concave shoulder, taper probe	400	450	Groove
2	15	750	Flat shoulder, cylindrical probe	410	545	Flash
3	20	750	Flat shoulder, taper probe	440	520	free
4	10	1000	Flat shoulder, cylindrical probe	425	480	free
5	15	1000	Flat shoulder, taper probe	395	470	crack
6	20	1000	Concave shoulder, taper probe	475	515	free
7	10	1200	Flat shoulder, taper probe	465	450	crack
8	15	1200	Concave shoulder, taper probe	460	560	Crack
9	20	1200	Concave shoulder, cylindrical probe	500	500	Tunnel

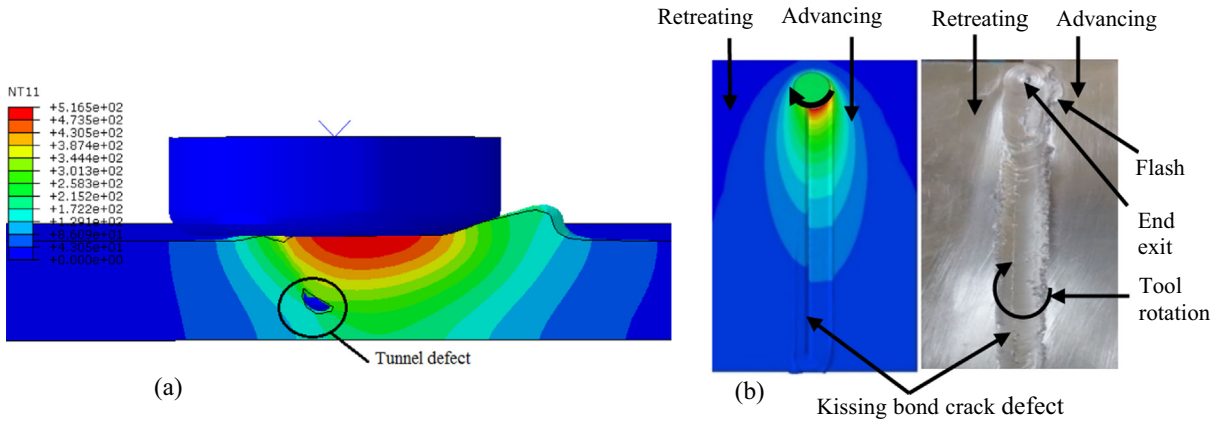

Fig. 9. FSW defects (a) Tunnel Defect (b) crack and kissing bond defects.

such as tunnel, crack and kissing bond are shown in Fig. 9 based on FE and experimental results.

4. Conclusions

A 3D Dynamic, Temp-disp, explicit with Johnson-Cook material model and CEL model was used to describe the FSW process of AA6061-T6. Abaqus software is a capable tool to simulate the FSW process, show material mixing flow, predict peak temperature and defect estimation. Tool geometry is a dominant factor for heat generation. Rotational speed and welding speed also affect the joint quality. The defect formation can be reduced by controlling rotational speed and other process parameters.

- The highest temperature was 560 °C which was observed at 1200-rpm rotational speed, 15mm/min. welding speed, concave shoulder, and taper probe. Kissing bond crack defects formed at this process parameters combination.
- A defect-free joint achieved at 750-rpm rotational speed, 20 mm/min welding speed, and Flat shoulder with taper probe.
- The best mesh size that gives a good result was 0.33 with reasonable running time.
- The lowest rotational speed and welding speed results in defects like groove whereas the highest rotational speed results tunnel defect.
- Flat shoulder is the best tool to reduce tunnel defects and concave shoulder reduce excessive flash defects.
- The temperature result from software comparatively higher than experimental.
- Excessive flash more likely happen when tool shoulder is flat than concave shoulder.

CRediT authorship contribution statement

Lingerew E. Melaku: Investigation, Software, Conceptualization, Methodology, Resources, Writing – original draft. **Amanuel D. Tura:** Data curation, Conceptualization, Methodology, Resources, Writing – original draft. **Hana B. Mamo:** Software, Data curation, Formal analysis, Resources. **A. Johnson Santhosh:** Software, Data curation, Resources. **N. Ashok:** Validation, Supervision.

Declaration of Competing Interest

The authors declare that they have no known competing financial interests or personal relationships that could have appeared to influence the work reported in this paper.

Funding Information

Funding granted to Corresponding Author: Lingerew E. Melaku by Jimma Institute of Technology under Mega Project Code: JiT_2021_22, Ref. No: RPD/JiT/327/14 dated 07/02/2022.

References

[1] P. Pradeep Kumar, S.A. Basha, S. Sai Kumar, Optimization of Friction Stir Welding process parameters of Aluminium alloy AA7075-T6 by using Taguchi method, Int. J. Innov. Technol. Exploring Eng. (IJITEE) 8 (12) (2019) Oct.
[2] G. Shinde, S. Gajghate, P. Dabeer, C. Seemikeri, Low cost friction stir welding: a review, Mater. Today:. Proc. 4 (Jan. 2017) 8901–8910.

[3] K. Li, F. Jarrar, J. Sheikh-Ahmad, F. Ozturk, Using coupled Eulerian Lagrangian formulation for accurate modeling of the friction stir welding process, Procedia Eng. 207 (2017) 574–579.
[4] H. Schmidt, J. Hattel, J. Wert, An analytical model for the heat generation in friction stir welding, Modell. Simul. Mater. Sci. Eng. 12 (1) (2004) 143–157.
[5] R. Kovacevic, Welding processes, BoD – Books on Demand (2012).
[6] Mohammad Kazem, Besharati Givi, and Parviz Asadi, Advances in Friction-Stir Welding and Processing, 1st ed., vol. 1. 2014.
[7] M. Đurđanović, M. Mijajlović, D. Milčić, and D. Stamenković, "Heat Generation During Friction Stir Welding Process," vol. 31, Jan. 2009
[8] S. Ismail, Finite Element Analysis (FEA) on Friction Stir Welding of Aluminium Alloy, AA5083 Using Coupled Eulerian-Lagrangian Model with Time-Scaling, IRC, UTP, Jan. 2020.
[9] N. Dialami, M. Cervera, M. Chiumenti, Defect formation and material flow in friction stir welding, Eur. J. Mech. A. Solids 80 (Mar. 2020) 103912.
[10] H. Agha Amini Fashami, N. Bani Mostafa Arab, M. Hoseinpour Gollo, B. Nami, Numerical and experimental investigation of defects formation during friction stir processing on AZ91, SN Appl. Sci. 3 (1) (2021) 108.
[11] F. Ducobu, E. Rivière-Lorphèvre, M. Galindo-Fernandez, S. Ayvar-Soberanis, P.-J. Arrazola, H. Ghadbeigi, Coupled Eulerian-Lagrangian (CEL) simulation for modelling of chip formation in AA2024-T3, Procedia CIRP 82 (2019) 142–147.
[12] N. Dialami, M. Chiumenti, M. Cervera, C. Agelet de Saracibar, Challenges in thermo-mechanical analysis of friction stir welding processes, Arch. Computat. Methods Eng. 24 (1) (2017) 189–225.
[13] Q. Weaver, "Numerical modeling and validation for the development of tool geometry and material for friction stir welding of thick copper" 2017.
[14] Sanjeev N K and Ravikiran B P, "Application of Coupled Eulerian Lagrangian Approach in Finite Element Simulation of Friction Stir Welding," 2016.
[15] D. Veljic, P. Milenko, A. Sedmak, M. Rakin, Numerical simulation of the plunge stage in friction stir welding alloys EN AW 2024 T 351 and EN AW 7049A T 652, J. Technol. Plasticity 36 (2011) Jan.
[16] Alvaro Jose Martinez and Maria Romero Menendez, "METALLIC PLASTICITY MODELLING – ABAQUS FEM CODE", icemm, 2016.
[17] R. Jain, S.K. Pal, S.B. Singh, "Numerical modeling methodologies for friction stir welding process", in computational methods and production engineering, J. Paulo Davim, Ed. Woodhead Publishing (2017) 125–169, https://doi.org/10.1016/B978-0-85709-481-0.00005-7.
[18] G. Mathers, The Welding of Aluminium and Its Alloys, 1st edition. Boca Raton, Fla.: Woodhead Publishing, 2002.
[19] A. Subburaj, R. Durairaj, A. M. M. A. J. Decruz, and V. K. Dharmaraj, "PROCESS-PARAMETER OPTIMIZATION OF WEDM WITH INCONEL 825 ALLOY USING GRA," Materials and Technology, vol. 55, no. 2, Art. no. 2, Apr. 2021.
[20] B.M.A. Al Bhadle, R.A.A. Al Azzawi, R. Thornton, K. Beamish, S. Shi, H.B. Dong, Equations of heat generation during friction stir welding for tapered polygonal tools, Sci. Technol. Weld. Joining 24 (2) (Feb. 2019) 93–100.
[21] Y. Zhao, J. Han, J.P. Domblesky, Z. Yang, Z. Li, X. Liu, Investigation of void formation in friction stir welding of 7N01 aluminum alloy, J. Manuf. Process. 37 (2019) 139–149.